Rheo-dielectric study of MXenes-based Pickering emulsions

Benedetta Attaianese[†] and Ruth Cardinaels[*,†,‡]

[†]*Soft Matter Rheology and Technology, Department of Chemical Engineering, KU Leuven, Celestijnenlaan 200J, 3001, Leuven, Belgium*

[‡]*Processing and Performance of Materials, Department of Mechanical Engineering, TU Eindhoven, P.O. Box 513, 5600 MB, Eindhoven, the Netherlands*

E-mail: ruth.cardinaels@kuleuven.be

Phone: +32 16 32 16 88

Abstract

Using MXene nanosheets as stabilizers in emulsion-templating offers a promising route for fabricating conductive composites with low percolation thresholds. The MXene network formed at the droplet interfaces, combined with the emulsion microstructure, gives rise to a gel-like material exhibiting strong electrical percolation. This study unravels the relationship between, on the one hand, the microstructure and, on the other hand, the viscoelastic and functional properties of MXene-stabilized emulsions. This is achieved by combining interfacial and bulk characterization techniques, including interfacial and bulk rheology, broadband dielectric spectroscopy, and microscopy. Interfacial measurements revealed a clear link between the rheological behavior and electrical conductivity of the MXene interfacial network. In the bulk, the characterization of MXene-based Pickering emulsions showed that the overall conductivity depends on both the interfacial network and the droplet-droplet interactions. Finally, through

rheo-dielectric and rheo-optical characterizations, we demonstrate that the emulsion microstructure influences the electrical conductivity and rheological properties of MXene-stabilized emulsions under shear flow and their recovery after shear.

Introduction

Pickering emulsion templating represents a versatile and effective approach for fabricating functional materials with tailored structures and properties.[1,2] The use of interfacially active particles allows the design of emulsions with enhanced stability and viscoelastic properties. Additionally, the choice of particles can also endow the final material with specific functionalities. In this context, two-dimensional particles, so called nanosheets, have attracted growing interest as Pickering stabilizers due to their unique properties such as a large surface area, good mechanical strength and the availability of conductive variants.[3,4] Among these, MXenes and particularly $Ti_3C_2T_X$, have emerged as a promising class of materials for formulating conductive and mechanically stable emulsions. MXene-stabilized emulsions have mostly been exploited as a template for the fabrication of porous composites with a segregated conductive network that reduces the particle percolation threshold.[5–8] These templating routes have recently been extended towards direct ink writing (DIW) printing, where nanosheet-based emulsions behave as gel-like printable inks that can retain shape fidelity while enabling controlled formation of percolated conductive networks.[9,10]

While most studies have focused on optimizing the conductivity and mechanical strength of the final porous composites, little attention has been devoted to understanding the fundamental properties of the MXene-stabilized emulsion itself. Yet, the mechanical and electrical behavior of the final material originates directly from the multiscale structure of the emulsion. In particular, the emulsion properties are linked to the internal structure on two distinct scales: the interfacial and the droplet networks.

At the interface, the viscoelastic and electrical properties are determined by the interfacial activity of the nanosheets and their assembly mechanism at the oil-water interface. Although

as-synthesized $Ti_3C_2T_X$ MXenes are highly hydrophilic and weakly surface active, interfacial assembly can be promoted through surface modification or electrostatic complexation with surfactants.[11–14] Our previous work demonstrated that MXene-PDMSNH_2 complexes form a robust interfacial layer with a percolated viscoelastic interfacial network. Similar interfacial percolation phenomena have been reported for other 2D materials such as graphene, for which Blair et al. reported that interfacial electrical and mechanical percolation are strongly related.[15] Namely, a conductive interfacial network is formed when the nanosheets transition from unconnected particle islands to a highly interconnected particle layer. More recently, Popple et al. demonstrated that the MXene interfacial layer between water and toluene can also create a strong conductive network, with the deposited film reaching DC conductivity values up to approximately 100 S/cm.[16]

On a larger scale, the droplet network also plays a key role in the bulk viscoelastic and electrical properties of Pickering emulsions. The rheological properties of Pickering emulsions have been broadly studied over the years for a wide range of particle stabilizers.[17] The interfacial viscoelastic network promotes the formation of solid-like droplets with high resistance to flow-induced deformation.[18] At high volume fractions of the dispersed phase, high internal phase emulsions (HIPEs) are formed, in which droplets are densely packed and form a mechanically percolated network. This jammed structure confers high elasticity and gel-like behavior to the material, whether stabilization is achieved by interfacial films alone or is reinforced by a viscoelastic particle network in the bulk.[19,20] The rheological properties of emulsions with nanosheet stabilizers, such as MXenes or graphene oxide (GO), have mostly been studied to investigate the printability of the emulsion ink.[9,21] Nanosheet-based emulsions exhibit all the key rheological attributes for good printability:[20] gel-like behavior with a yield stress, shear thinning, and rapid recovery. However, despite the growing use of nanosheet-based emulsions as printable gels, the links between their bulk rheological properties and their electrical conductivity, together with those between their bulk and interfacial properties, remain unexplored. Understanding these relationships is crucial for

rational formulation of conductive inks and for moving beyond the current trial-and-error optimization strategies.

In this work, we address this gap by investigating the multiscale coupling between interfacial and bulk properties in conductive MXene-stabilized Pickering emulsions. First, we probe the interfacial rheological and electrical behavior of MXene-surfactant complexes at water-dodecane interfaces using shear interfacial rheometry and four-point probe conductivity measurements. We then characterize the internal microstructure and dielectric response of the emulsions both in static conditions and under flow using confocal microscopy, oscillatory rheology, and broadband dielectric spectroscopy (BDS). This study provides new insights into the hierarchical structure-property relationships in MXene-based Pickering emulsions and establishes a framework for designing conductive multiphase materials based on conductive nanosheets.

Experimental section

Materials

Ti_3AlC_2 MAX phase with particle size $\leq$ 40 μm was purchased from Carbon Ukraine. $Ti_3C_2T_X$ MXene sheets, where T_X denotes surface termination groups (e.g., -O, -OH, -F) introduced during the synthesis, were synthesized using an adapted MILD method[22] as described in our previous work[23] and dried according to the procedure developed by Seok et al.[24] The particles were characterized by performing SEM/EDX, XRD, AFM and DLS, exhibiting an average lateral size of 205.3 $\pm$ 2.2 nm and a height around 2nm. Detailed characterization results are available in our previous work.[23] MXene aqueous suspensions were prepared by suspending dried MXene nanosheets in MilliQ water with a concentration between 5 mg/mL and 15 mg/mL in an ultrasonic bath (Elmasoni S 30 H, 80W) for 5 minutes. n-Dodecane (99%, Thermo Fisher Scientific) was used as the oil phase with the addition of biaminopropyl-terminated polydimethylsiloxane ($PDMSNH_2$, SigmaAldrich,

M_W=2500 g/mol) cationic surfactant. Nile red (Sigma Aldrich) was used as a fluorescent dye for the oil phase. MilliQ water (Sartorius Stedim Arium 611DI, conductivity 0.055 $\mu S/cm$) was used to prepare the aqueous phase.

Interfacial shear rheology

The interfacial shear rheological properties of water-dodecane interfaces were determined with a double wall-ring geometry (DWR) attached to a stress-controlled rheometer (DHR-3, TA Instruments), as also described in our previous study.[23] The evolution of the interfacial network assembly was monitored by performing time sweep tests at 1 rad/s with a 0.01% strain for 1 hour, after which steady state was reached. The viscoelastic properties of the interface were then assessed by performing frequency sweeps from 10^{-1} rad/s to 10^{1} rad/s at 0.01% strain to keep the sample in the linear region and an amplitude sweep from 0.001% to 100% strain at 1 rad/s.

Film deposition and conductivity measurements

Flat water-dodecane interfaces stabilized by MXene-PDMSNH_2 were prepared in a petri-dish containing a glass substrate at the bottom (size 1.5cmx1.5cm). After one hour, the MXenes interfacial network was gently deposited by slowly lifting the substrate. The coated substrates were left to dry overnight in a vacuum oven. To keep part of each substrate uncoated, the borders were masked with tape that was removed after the film deposition. Finally, the conductivity of the films was measured using a four-point probe setup (Ossila), where the conductivity $\sigma = 1/(R_s \cdot t)$, whereby R_s is the sheet resistance given by the device, while t is the thickness of the films. The latter was measured using a profilometer (Dektak XT, Bruker) by determining the height difference between the uncoated borders of the substrate and the coated center. Each measurement was repeated five times at different locations on the substrate to ensure reproducibility.

Emulsion preparation and characterization

The oil phase was prepared by mixing dodecane with $PDMSNH_2$ at different concentrations between 0.25wt% and 2wt%, and Nile Red at 0.05 mg/mL. The aqueous suspension was then added in steps of 100 μL to the oil phase under continuous stirring with a magnetic stirrer at 1700 rpm until a total volume of 2 mL was reached. Once the aqueous phase had been fully added, the sample was further mixed for an additional 15 minutes. The volume fraction of the aqueous phase in the emulsion was varied between 0.6 and 0.8.

Confocal microscopy images of the prepared emulsions were taken using a Leica TCS SP8 inverted confocal laser scanning microscope with a 20x/0.75 glycerol immersion objective. A solid state laser with a wavelength of 488 nm was used for the excitation of the Nile Red dye. The emission signal was collected between 550 nm and 700 nm. Images were acquired at multiple locations to ensure sample homogeneity. The droplet size distribution and droplet aspect ratio were determined by analyzing the confocal images using ImageJ. Morphological filtering implemented in the MorphoLibJ plugin was applied to enhance the contrast between the droplet and matrix phases. A total of 100-150 droplets were analyzed for each sample.

The dielectric properties of the emulsions were characterized using a Novocontrol Alpha Analyzer coupled to a MCR501 stress-controlled rheometer (Anton Paar). Broadband dielectric frequency sweep (BDS) measurements were performed in static conditions, placing the emulsion sample between 25 mm diameter parallel plates with 1 mm thickness in a frequency range from 10^{-2} Hz to 10^{7} Hz at room temperature. All dielectric quantities reported (ε', ε'', ε^*, M', M'') are expressed relative to the permittivity of free space, ε_0. Figure S1 verifies the reproducibility of the dielectric data, showing consistent results across three repeated measurements.

The same rheometer was used to perform oscillatory rheological measurements. Frequency sweeps were performed at 0.1% strain between 0.1 and 100 rad/s, while amplitude sweeps were perfomed at 1 rad/s with a strain between 0.01% and 1000%. Figure S2 presents the reproducibility of the shear rheological data, confirming good agreement among three

repeated measurements. Additionally, we performed dielectric measurements under oscillatory flow. The electric field was applied at a frequency of 1 Hz and the conductivity was monitored over time during oscillatory shear flow at 1 rad/s with a strain between 0.01% and 1000%. To prevent any interference in the rheological measurements from the electrical connections to the dielectric analyzer, the rheological and dielectric data were collected in separate experiments.

All measurements were performed on freshly prepared emulsions after a 10 minutes equilibration period. Time sweep measurements showed that the storage and loss moduli reached a plateau after the 10 minutes equilibration period (Figure S3) and confocal imaging performed in parallel on part of the sample confirmed the absence of coalescence or macroscopic structural evolution over the experimental timescale.

The evolution of the emulsion microstructure under oscillatory shear flow was also monitored using a rheo-optical setup consisting of a double motor stress-controlled rheometer (MCR702, TA Instruments) equipped with two glass plates and coupled with a stereo microscope.[25] The rheo-optical measurements were performed using 43 mm diameter parallel plates with a gap of 1 mm. The emulsions were sheared at 1 rad/s with a strain between 0.01% and 1000% while imaging their microstructure under flow in the velocity-vorticity plane.

Results and discussion

Properties of MXene-covered interfaces

In our previous work, we investigated in detail the interfacial rheological properties of MXene-$PDMSNH_2$ complexes at water-PDMS interfaces in excess of cationic surfactant.[23] MXenes alone exhibit weak interfacial activity and interfaces covered only by $PDMSNH_2$ show weak viscoelasticity. However, their electrostatic interaction allows the formation of a viscoelastic interfacial layer. According to our findings, the electrostatic interaction between MXene

and $PDMSNH_2$ and, therefore, their interfacial assembly result in the formation of a gel-like interfacial network. The interfacial viscoelastic properties are highly dependent on the MXene concentration, with the interfacial elastic moduli increasing with the increase of MXene bulk concentration.[23] In the present study we explore the effect of the surfactant-to-MXene weight ratio (S/M) on the interfacial rheological properties. Figure 1a shows the interfacial frequency sweep of MXene-covered interfaces at different S/M ratios with a fixed MXene concentration of 5 mg/mL. All samples show a higher storage modulus (G') than loss modulus (G") across the tested frequency range, indicating dominant elastic behavior. The storage and loss moduli increase with the increase of the S/M ratio, indicating the formation of a stronger interfacial network. At S/M = 0.5, G' and G" nearly intersect around $\omega = 0.1\ rad/s$, suggesting a transition towards viscoelastic liquid behavior at low frequencies. In contrast, at S/M = 2, both moduli exhibit similar slopes without crossover, reflecting a more elastic and stable interfacial network. From the amplitude sweep measurements (Figure S4), the critical strain and crossover point remain essentially unchanged with surfactant concentration, suggesting that the yielding mechanism of the interfacial network is not significantly affected by the S/M ratio. Therefore, the surfactant concentration influences the elasticity of the interfacial network but not its brittleness, which appears to be governed primarily by particle-particle interactions.

This was also confirmed by measuring the thickness of the interfacial layer by depositing the film at the water-dodecane interface on a glass substrate (Figure 1b). While the thickness of the film slightly increases with the concentration of MXene (between 1 and 2.5 μm), it does not change significantly with the S/M ratio. This suggests that the increase of surfactant concentration promotes the formation of a more interconnected network rather than the stacking of additional layers of MXene at the interface. The total amount of MXene available in the bulk phase would be sufficient to form approximately 2000-4000 layers at the water-dodecane interface. However, based on the measured film thickness (corresponding to roughly 500-1250 layers), only about 25% of the available MXene is effectively assembled at

the interface.

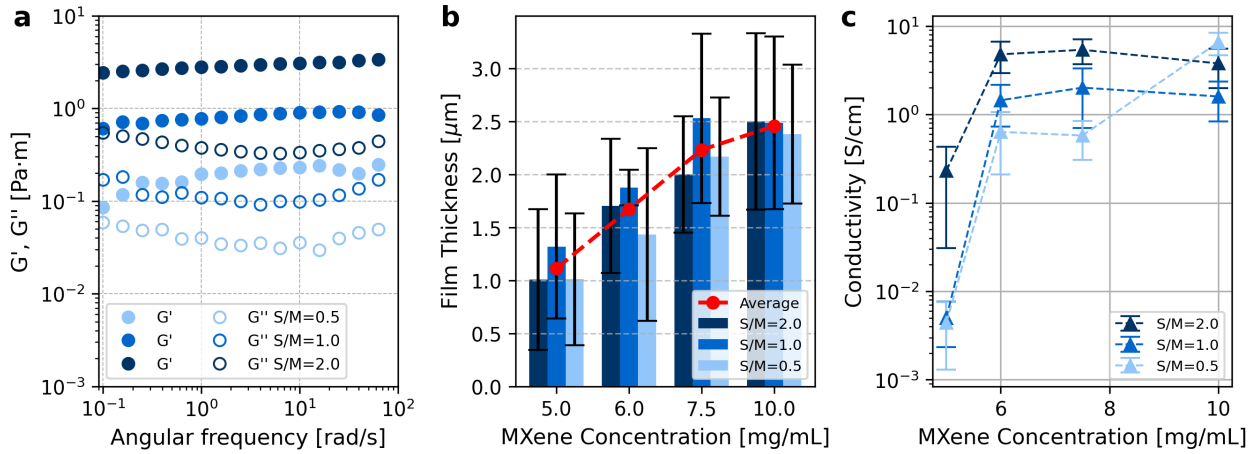

Figure 1: (a) Interfacial frequency sweep of MXene-covered interfaces at different S/M (S=PDMSNH$_2$ - M=$Ti_3C_2T_X$). The MXene concentration is fixed at 5 mg/mL. (b) Thickness of deposited MXene-PDMSNH$_2$ layer versus MXene bulk concentration at different S/M ratios. (c) Conductivity of deposited MXene-PDMSNH$_2$ layer versus MXene bulk concentration at different surfactant to MXene ratios (S/M).

Finally, we investigated the conductivity of the deposited interfacial film by 4-point probe measurements for different concentrations of MXenes and S/M ratios (Figure 1c). Previous studies have already reported the formation of conductive nanosheet-based films via interfacial deposition,[15,16,26] demonstrating that electrical percolation can be achieved through uniform surface coverage with high interflake contacts, even in films with only a few nanosheet layers. For MXene films deposited from water-dodecane interfaces, the film conductivity initially increases with the MXene concentration and then reaches a plateau, which can be attributed to the saturation of the interfacial coverage. The sheet conductance ($1/R_S$) also shows a plateau at high MXene concentrations (Figure S5). This behavior suggests that once a continuous conductive pathway is established and the interface becomes effectively saturated with nanosheets, further MXene addition mainly increases film thickness rather than creating additional conductive pathways, resulting in the observed conductivity plateau. In contrast, the S/M ratio has a significant effect on the film conductivity: increasing the surfactant concentration enhances nanosheet connectivity at the interface, leading to an in-

crease in conductivity by up to one order of magnitude. This behavior is consistent with the interfacial shear rheology results, which show the formation of a more viscoelastic interfacial network at higher S/M ratios.

Properties of conductive emulsions stabilized by MXene-PDMSNH$_2$

To gain a deeper understanding of the structure-properties relationships in MXene-PDMSNH$_2$ complexes on a larger scale, we investigated the rheological and conductive properties of emulsions stabilized by MXenes and PDMSNH$_2$. In the bulk system, interfacial conductivity is not the only contribution to charge transport. As shown in Figure 1, MXene-surfactant complexes assembled at the droplet interface form a conductive nanosheet network whose intrinsic conductivity is determined by the connectivity of MXene nanosheets within the interfacial layer. However, in the emulsion, macroscopic charge transport requires that these conductive interfaces are connected through the droplet network. Therefore, the bulk electrical conductivity does not depend solely on the properties of individual interfaces, but also on the degree of droplet-droplet connectivity that enables long-range percolation across the sample. As a result, the interfacial conductivity and the droplet network represent two distinct but coupled mechanisms governing electrical transport in MXene-stabilized emulsions.

In the following sections, we will first discuss the effect of the volume fraction of the dispersed phase on the droplet network and its impact on the rheological and dielectric properties of the emulsions. We then examine the effects of the S/M ratio and the MXene concentration. Finally, we will discuss the coupling between rheology and dielectric properties of the emulsions under flow.

Effect of the volume fraction of the dispersed phase

Figure 2 shows the results for water-dodecane emulsions with a fixed MXene concentration of 5 mg/mL and S/M ratio of 2. The volume fraction of the aqueous phase was varied between 0.60 and 0.80. From confocal microscopy images (Figure 2a), it is clear that, at low

volume fraction ϕ_w, the droplets have a low interfacial contact area. Increasing the volume fraction ϕ_w leads to jamming and deformation of the droplets towards a structure similar to that of high internal phase Pickering emulsions (HIPPEs). However, at $\phi_w = 0.80$, the droplets appear again less confined. This behavior may result from the broader droplet size distribution observed for this sample (Figure 2b), which can reduce packing homogeneity even at high overall volume fraction. This polydispersity also leads to a higher maximum packing factor,[27] resulting in lower confinement. This results in a weaker mechanical network, as shown in the shear rheological results. All the samples show a gel-like behavior with G'>G" in the whole frequency range (Figure S6). However, G' and G" initially increase with ϕ_w, but their values suddenly drop at $\phi_w = 0.80$ (Figure 2c), confirming the formation of a less mechanically stable network. The amplitude sweep results show a weak two-step yielding behavior at low water volume fraction ($\phi_w = 0.6$), as indicated by the presence of two small G" peaks (Figure 2c), while the intersection of G' and G" corresponds to the strain at which the elastic and viscous responses become comparable, marking the onset of structural rearrangement of the droplet network. The crossover strain increases with increasing ϕ_w, indicating that a progressively larger deformation is required to initiate irreversible flow. This may be caused by the fact that a more dense packing hinders the flow of droplets past each other. At higher ϕ_w, the two-step yield disappears, and G" exhibits a single overshoot around $\gamma = 1\%$. As suggested by Zhou et al.,[28] the two G" peaks can orginate from an initial breakup of droplet-droplet interactions followed by droplet rearrangement during which the droplets collide with each other, generating energy dissipation and, therefore, the second peak. At higher ϕ_w, the free volume decreases and droplets can only partially rearrange leading to a single-step yielding behavior. A similar behavior has been reported by Fuhrmann et al.[29] for emulsions with electrostatically attractive droplet interactions. This suggests that the droplet interactions are predominantly attractive, arising either from surfactant bridging between MXene-coated interfaces, enabled by the double amino termination of $PDMSNH_2$,[30] or from surfactant-induced depletion attraction due to excess surfactant in

the bulk phase.[31] At the same time, short-range repulsive forces can originate from steric hindrance of the adsorbed surfactant layers and from electrostatic repulsion between similarly charged MXene-surfactant interfaces.

Taken together, these rheological results indicate that the emulsions form a mechanically percolated droplet network whose connectivity and stability strongly depend on ϕ_w. Because electrical transport in these systems is mediated by the conductive MXene-coated interfaces as well as the droplet-droplet contacts, the same structural connectivity that governs the mechanical response is also expected to control the emergence of long-range electrical pathways. To directly probe this structure-conductivity relationship, we next characterize the frequency-dependent dielectric and conductive response of the emulsions by BDS measurements. Broadband dielectric spectroscopy has been widely used to study the dielectric and conductive mechanisms of polymer composites.[32,33] Biphasic systems, such as those containing spherical inclusions dispersed in a matrix, can exhibit a dielectric relaxation peak arising from interfacial polarization, also known as Maxwell-Wagner-Sillars (MWS) polarization. This phenomenon is mainly governed by the dielectric constants and conductivities of the two phases, as well as the volume fraction of the dispersed phase.[34] Simple biphasic systems, including polymer blends[35] and polymer composites with a low concentration of conductive fillers,[36] typically display an MWS relaxation in their dielectric spectra, along with possible relaxations associated with the individual phases. Instead of being in direct contact, particles are often covered with a thin adsorbed polymer layer, creating a thin inter-particle gap, which can be modelled as a resistor and capacitor in parallel.[37] More complex multiphase systems, such as Pickering emulsions, can exhibit an even richer dielectric response arising from multiple interactions among the various phases present in the sample. In such systems, electrical transport may occur through a combination of direct particle/droplet contacts and electron hopping or tunneling through a thin inter-droplet gap, and the effective conductivity becomes strongly dependent on network connectivity.

For MXene-stabilized emulsions with a MXene concentration of 5 mg/mL, all samples

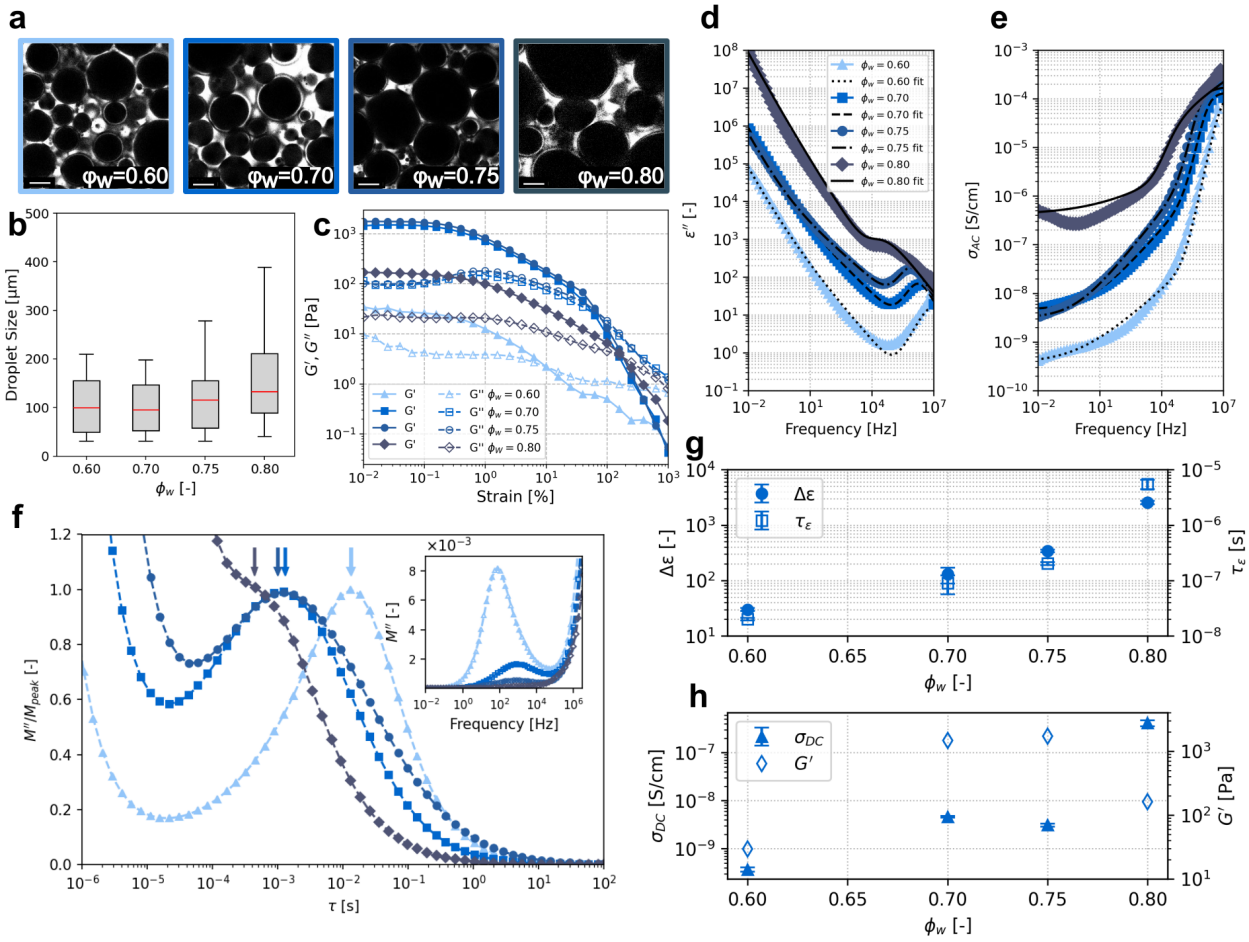

Figure 2: Water-dodecane emulsions with 5 mg/mL of MXenes and S/M=2 (S=PDMSNH$_2$ - M=$Ti_3C_2T_X$) for different water volume fractions ϕ_w between 0.6 and 0.8. (a) Confocal images. Scale bar is 100 μm. (b) Droplet size distribution versus water volume fraction. (c) Shear amplitude sweep at $\omega = 1\ rad/s$. (d) Dielectric loss ε'' and (e) AC conductivity σ_{AC} versus frequency. The lines represent the fits obtained from Eq. 1. (f) Normalized electric modulus M" versus oscillation period. The arrows indicate the main relaxation peak for each sample. Inset: M" versus frequency. (g) Dielectric strength $\Delta\varepsilon$ and dielectric relaxation time τ_ε and (h) DC conductivity σ_{DC} obtained from Eq. 1 together with the LVE storage modulus G' at 1 rad/s as a function of water volume fraction ϕ_w. The error bars correspond to model uncertainty derived from the parameter covariance matrix of the nonlinear least-squares fit in Eq. 1.

exhibit a clear dielectric relaxation in the high-frequency region (Figure 2d and Figure S1). To identify the origin of this relaxation peak, dielectric measurements of the individual liquid phases were performed separately and are reported in Figure S7. Dodecane shows a constant ε' across the entire frequency range, with $\varepsilon' = 2$ in agreement with previous literature.[38] Adding $PDMSNH_2$ to the sample does not significantly change the dielectric response, which is expected since the amino-terminated polymer in a nonpolar environment cannot form strong dipoles, and thus no relaxation is observed. The water phase exhibits pronounced electrode polarization at low frequencies, probably due to the conductive nanosheets and residual lithium ions from the nanosheet synthesis. At high frequencies, the dielectric response of the MXene suspension is dominated by its conductivity, with $\sigma_{DC} = 7.7 \cdot 10^{-4} S/cm$. Since neither of the liquid phases shows any relaxation in their dielectric spectra, the relaxation behavior observed in the emulsion samples can be attributed to interfacial MWS polarization, and therefore, charge accumulation at the droplet interface.[32]

The relaxation time, dielectric strength and conductivity of a sample can give more insight into the effect of the sample microstructure on its dielectric and conductive properties. Therefore, the data were further analyzed using the following equation for the complex permittivity ε^*:[39]

$$\varepsilon^* = \varepsilon_\infty + \frac{\Delta\varepsilon}{1 + (i\omega\tau_\varepsilon)^\alpha} - i\frac{\sigma_{DC}}{\varepsilon_0\omega} + \frac{B}{\varepsilon_0}(i\omega)^{n-1} \tag{1}$$

The complex permittivity consists of three different contributions: the dielectric interfacial MWS relaxation, a DC conductivity σ_{DC} and an extra dispersion process that is typical of conductive polymers and conductive particle-based composites.[39,40] For the dielectric relaxation term, ε_∞ represents the dielectric constant at high frequency, $\Delta\varepsilon = \varepsilon_s - \varepsilon_\infty$ is the dielectric strength, and τ_ε is the relaxation time. The parameters were obtained by nonlinear least-squares regression, minimizing the combined residuals of $\varepsilon'(\omega)$ and $\varepsilon''(\omega)$. To limit parameter compensation, all variables were restricted to physically meaningful ranges and the optimization was performed using a two-step strategy, consisting of a global search by differential evolution to obtain robust initial parameters, followed by local least-squares

refinement. In Figures 2d and 2e the experimental data and the corresponding fits for ε'' and $\sigma_{AC} = \varepsilon_0 \varepsilon'' \omega$ are reported. Additionally, a representation of the three different contributions of the model can be found in Figure S8. Focusing on the effect of ϕ_w on the dielectric properties, at $\phi_w = 0.60$, the dielectric strength $\Delta\varepsilon$ is in between the permittivity of dodecane and that of water (e.g. $\varepsilon'_d = 2$ and $\varepsilon'_w = 80$) indicating a not fully percolated network where droplets act more as isolated fillers. When $\phi_w > 0.60$, $\Delta\varepsilon > \varepsilon_d$ and ε_w, suggesting the presence of an additional contribution to the dielectric properties that can be attributed to the interaction between interfacial layers and the formation of a percolated network (Figure 2d). The corresponding relaxation time also increases with the increase of ϕ_w in accordance with the model proposed by Skodvin et al.,[41] which considers purely interfacial dielectric relaxation effects and does not include conductive contributions. According to the model, the relaxation time and dielectric strength $\Delta\varepsilon$ in water-in-oil emulsions increases with the increase of the dispersed phase volume fraction. This is caused by the increase of the total interfacial area that leads to a stronger interfacial polarization and, therefore, a higher $\Delta\varepsilon$. Conversely, a higher ϕ_w, the increasing droplet-droplet interactions promote interfacial charge accumulation and interfacial dipole reorientation across neighboring droplets, rather than independent polarization of isolated droplets. This collective interfacial polarization slows down the relaxation process as compared to more localized relaxations. Finally, the conductivity contribution increases with the increase of the aqueous phase volume fraction (Figure 2h). A typical variation in the extracted conductivity for independently prepared emulsions is on the order of half a decade. Therefore, the apparent decrease observed in Figure 2h at $\phi_w = 0.75$ falls within the experimental uncertainty. Since the emulsions are highly concentrated, they are likely well above the percolation threshold, and the measurements probe the post-percolation regime in which conductivity is governed by the structural evolution of the droplet network.[42] The conductivity increases gradually with ϕ_w, which can be attributed to the progressive densification and strengthening of the droplet network, whereby an increase of interfacial area and droplet-droplet interactions, combined with larger

droplet-droplet contact area's due to enhanced droplet packing increase the connectivity of the conductive network.

Additional information on the effect of ϕ_w on the conductivity mechanism of the sample can be obtained by analyzing the electric moduli $M^*(\omega) = 1/\varepsilon^*(\omega)$. The analysis of the electric moduli represents a useful tool to analyze the spectra of conductive materials since this representation enables to suppress the effect of electrode polarization (i.e. high ε^* value at low frequencies) and clearly reveals the conductive peak characteristic of the system.[43,44] Compared to the dielectric relaxation time τ_ε, the relaxation time τ_σ derived from the M" peak is related to the motion of charge carriers, while τ_ε represents the relaxation of dipoles which, for our system, results from the polarized droplet interface. In systems that present both a conductive and a dielectric relaxation, M" should include two relaxation peaks at τ_ϵ and τ_σ.[45] In our system, it is difficult to distinguish the dielectric relaxation from the M" plot since this appears at high frequencies where M" start to diverge (Figure 2f). Only for $\phi_w = 0.80$, it is possible to distinguish the double relaxation since the dielectric relaxation is slower than in the other samples ($\tau_\varepsilon = 5.5 \cdot 10^{-6}$ s) (Figure S9). In general, τ_σ shows an opposite trend compared to τ_ε, decreasing with the increase of ϕ_w. This is due to the fact that increasing the water volume fraction increases the droplet-droplet contacts in the sample, thereby promoting the formation of additional pathways for charge hopping and, therefore, improving the conductivity mechanism. This observation is further supported by the trend in the magnitude of the M'' peak (inset of Figure 2f). At $\phi_w = 0.60$, the droplets form only a few contacts, and M" has a higher magnitude, indicating more localized charge motion. As ϕ_w increases, the M" peak decreases dramatically, suggesting the formation of a more interconnected droplet network throughout the sample.[32]

Interfacial conductivity contribution

To gain further insight into the interfacial contribution in the bulk electrical transport, the theoretical interlayer model proposed by Steeman et al.[46] was applied to our emulsion

system. In this model, the complex permittivity of a three-phase system consisting of a matrix, dispersed phase, and an interlayer is expressed as:[46]

$$\varepsilon_b^*(\omega) = \frac{\varepsilon_d^*(\omega)\phi_d + \varepsilon_i^*(\omega)\phi_i R + \varepsilon_m^*(\omega)\phi_m S}{\phi_d + \phi_i R + \phi_m S} \tag{2}$$

$$R = \frac{(1-n)\varepsilon_i^*(\omega) + n\varepsilon_d^*(\omega)}{\varepsilon_i^*(\omega)} \tag{3}$$

$$S = \frac{(n\varepsilon_i^*(\omega) + (1-n)\varepsilon_m^*(\omega))(n\varepsilon_d^*(\omega) + (1-n)\varepsilon_i^*(\omega)) + dn(1-n)(\varepsilon_i^*(\omega) - \varepsilon_m^*(\omega))(\varepsilon_d^*(\omega) - \varepsilon_i^*(\omega))}{\varepsilon_i^*(\omega)\varepsilon_m^*(\omega)} \tag{4}$$

$$d = \frac{\phi_d}{\phi_d + \phi_i} \tag{5}$$

where ε_m^*, ε_d^*, and ε_i^* represent the complex permittivities of the matrix, dispersed phase, and interlayer, respectively, while ϕ_m, ϕ_d, and ϕ_i are their corresponding volume fractions. The parameter n is a depolarization shape factor that describes the effective geometry of the inclusions relative to the direction of the applied electric field.

The model assumes that the dispersed inclusions are fully embedded in the matrix phase and electrically isolated from each other. This assumption does not strictly apply to our emulsion system, where droplet-droplet contacts facilitate the formation of a percolated conductive network. To adapt the model, we assumed that the oil phase acts as the dispersed phase within a continuous aqueous matrix, while the interlayer corresponds to the MXene-surfactant interface forming around the droplets. This assumption is justified by the large contrast in electrical properties between the two bulk phases: the aqueous phase exhibits a much higher effective conductivity than the oil phase. Consequently, the electric field preferentially propagates through the aqueous domains, which therefore behave as the continuous medium from the perspective of charge transport. In contrast, the oil domains interrupt the

conductive network and can be regarded as dielectric inclusions. This assumption is further supported by the observation that applying the model to the inverse configuration yields predictions that deviate significantly from the experimental results.

The interfacial layer separating the two phases is assumed to be highly conductive, with negligible real permittivity ε':

$$\varepsilon_i^* = i\varepsilon_i'' = i\frac{\sigma_{i,DC}}{\varepsilon_0 \omega} \tag{6}$$

Under these assumptions, ε_b^* was estimated using the shape factor n, the interlayer conductivity $\sigma_{i,DC}$ and the disperesed phase volume fraction ϕ_d as free parameters. Since the matrix fraction ϕ_m was fixed during the fitting, ϕ_d and ϕ_i are directly correlated by ϕ_m+ϕ_d+ϕ_i=1. This approach allows quantification of the interfacial contribution to the overall dielectric response through $\sigma_{i,DC}$ and provides structural information about droplet connectivity through n and ϕ_d.

As a proof of concept, Figure 3a presents the experimental complex permittivity data and corresponding model fits for emulsions with aqueous volume fractions between 0.6 and 0.8. The model correctly predicts the behavior of the emulsions at high frequencies. However, deviations at low frequencies are observed, likely due to electrode polarization effects, which are not captured by the interlayer model. For all datasets, the shape factor converged to $n = 1$, corresponding to plate-like fillers oriented perpendicular to the electric field.[46] Because the interlayer is highly conductive, its complex permittivity is several orders of magnitude larger than that of the oil phase over the entire frequency range, i.e. $|\varepsilon_i^*| >> |\varepsilon_d^*|$. Together with the fitted value n=1, this leads to $R \approx 0$ in Eq. 3. This result aligns with the expected microstructure of the emulsions, where at high dispersed-phase fractions, droplets are separated by thin oil films (Figure 3b). The interfacial conductivity remains approximately constant, with an average value $\sigma_{i,DC} = 0.45\ S/cm$, suggesting that the intrinsic conductivity of the MXene-surfactant interfacial network is governed primarily by the particle concentration and S/M ratio, and is not affected by the bulk volume fraction. Thus, the observed increase

in overall emulsion conductivity with increasing water content arises mainly from improved droplet connectivity and percolation. Interestingly, the estimated $\sigma_{i,DC}$ is comparable to the conductivity σ measured via the four-point probe method on a deposited MXene-surfactant film with the same MXene bulk concentration and S/M ratio ($\sigma = 0.23\ S/cm$), reinforcing the physical validity of the model. The model predicts a significantly lower effective oil

Table 1: Fit parameters obtained from the interlayer model (Eq. 2) using the experimental data shown in Figure 3a

ϕ_m [-]	ϕ_d [-]	ϕ_i [-]	n [-]	$\sigma_{i,DC}$ [S/cm]
0.60	0.057	0.343	1	0.485
0.70	0.012	0.288	1	0.401
0.75	0.005	0.245	1	0.451
0.80	0.001	0.199	1	0.468

volume fraction ϕ_d than the actual oil content used experimentally ($0.2 \leq \phi_{oil} \leq 0.4$). This discrepancy likely reflects the fact that, in concentrated emulsions, the electrical response is dominated by the insulating gaps between droplets rather than by the total oil volume. As the aqueous MXene phase forms a percolated network, only the thin films at the droplet contacts contribute to the dielectric response. Consequently, the model captures an effective filler fraction smaller than the experimental one. Nevertheless, the model predicts a decrease in ϕ_d with increasing aqueous content, correctly reflecting the progressive compression of the droplets within the emulsion network. Additionally, the robustness of the fitted parameters was evaluated by varying independently the interfacial conductivity, dispersed phase fraction, and the shape factor (Figure S10). In the model fit, the interfacial conductivity mostly determines the high frequency dielectric response. Increasing or decreasing the interfacial conductivity value with a factor two, leads to significant discrepancies between the experimental data and the model fit (Figure S10a), thereby demonstrating the robustness of the derived model parameters. As mentioned above, the model was also applied to the inverse configuration where the oil represents the continuous phase. In this case, the model fails to reproduce the experimental dielectric response showing a plateau at low frequencies (Figure

S11). Moreover, the fitted parameters become non-physical: the fitted dispersed-phase fraction tends to zero ($\phi_d \to 0$), and the model assigns all non-matrix volume to the interlayer, while simultaneously yielding an unrealistically high interfacial conductivity.

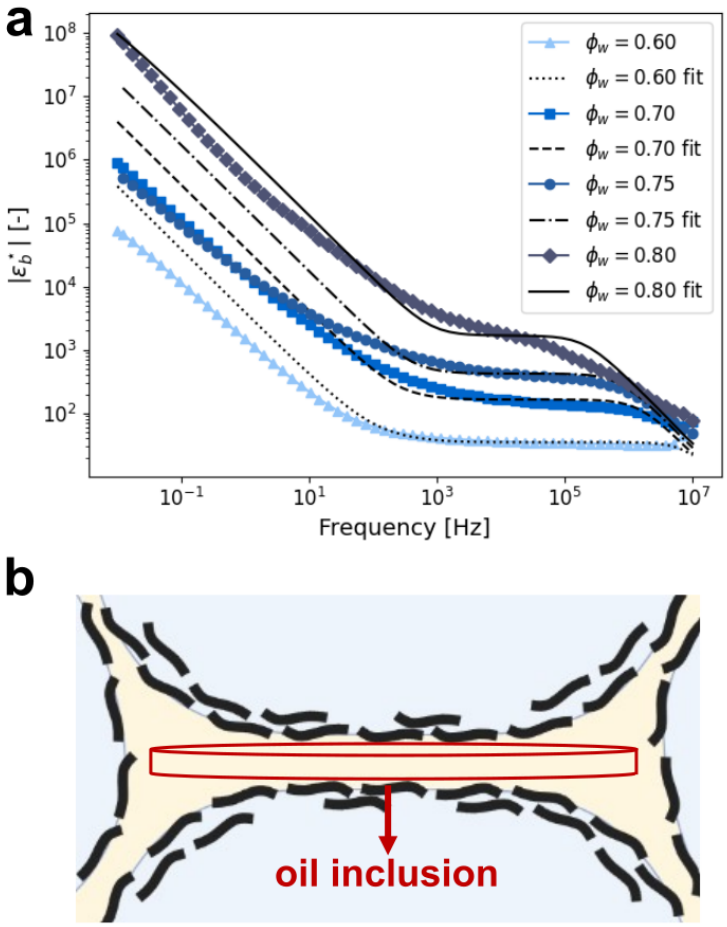

Figure 3: (a) Complex permittivity ε^* of MXene-stabilized emulsions with ϕ_w between 0.60 and 0.80 and S/M=2 (S=PDMSNH$_2$ - M=$Ti_3C_2T_X$). The lines represent the fits obtained using the interlayer model (Eq. 2). (b) Schematic of the proposed emulsion structure used in the interlayer model.

Effect of the surfactant-to-particle ratio

The effects of the surfactant-to-particle ratio on the rheological and electrical properties of the emulsions were investigated by keeping the concentration of MXene fixed at 5 mg/mL and varying the concentration of PDMSNH$_2$, allowing the role of the relative S/M ratio to be assessed independently from changes in conductivity arising from variations in particle

loading. As mentioned above, from the shear interfacial rheology measurements in Figure 1, it is clear that an excess of surfactant promotes the formation of a mechanically stronger and electrically better conductive interfacial network. However, a different and more complicated trend can be observed in the case of the biphasic system. It is worth mentioning that, in all the tested sample, the concentration of surfactant was always kept above the critical micelle concentration (CMC) measured by surface tensiometry (Figure S12). At S/M=0.5, the emulsion appears unstable with the droplets forming clear agglomerates and visible coalesced droplets (Figure 4a). This is caused by a weak interfacial network that also translates into weak viscoelastic properties of the emulsion (Figure 4b). At S/M≥1, the emulsion shows individual droplets without visible agglomeration or droplet coalescence. However, unlike the monotonic increase observed at the interface, the bulk storage and loss moduli do not increase continuously with S/M. Instead, G' and G" in the linear region present a maximum at S/M = 1. Similar observations were made by Li et al.,[9] who studied the printability of MXenes-based emulsion gels. The emulsions exhibited a self-supporting behavior (i.e. G'>G" and high yield stress) only for a S/M ratio close to 1. This rheological behavior is also similar to that of carbon black conductive suspensions, where surfactant is added to improve particle dispersion.[47,48] When the S/M ratio reaches a critical value, carbon black suspensions transition from a gel-like material to liquid-like behavior. This is caused by the formation of a surfactant layer on the carbon black that hinders particle-particle interactions and, therefore, the formation of a continuous network. A similar mechanism can also be applied for our emulsion system, where an excess of surfactant, which is in the matrix phase, can create repulsion between droplets. Additionally, dynamic light scatteing (DLS) measurements on the oil phase reveal that the increase of surfactant concentration leads to an increase of the size of the $PDMSNH_2$ agglomerates in the dodecane (Figure S13). The observed agglomerate size (300 nm-1 μm) is significantly larger than that of individual surfactant molecules (approximately 2 nm) and typical micelles, which generally do not exceed 100 nm in diameter.[49] This pronounced increase in size can be attributed to

the telechelic structure of the surfactant, which possesses two terminal amino groups. These functional end groups enable micelles to interconnect through bridging interactions between the surfactant terminations, leading to the formation of larger agglomerated structures.[50]

The S/M ratio influences not only the rheological response of the sample but also its dielectric behavior, as shown in Figure 4c-g. In contrast with the trend at the interface, where conductivity increases with S/M, the bulk emulsion conductivity decreases with the increase of the S/M ratio (Figure 4d). This confirms that, while excess surfactant strengthens interfacial connectivity, it hinders the formation of a conductive droplet network in the bulk, reducing the electrical conductivity of the system, as also seen in carbon black suspensions.[48] Conversely, the dielectric properties, fitted with Eq. 1, show that the dielectric strength $\Delta\varepsilon$ and dielectric relaxation time τ_ε are not significantly affected by the variation of surfactant concentration. This indicates that the droplet interaction has a minor effect on the interfacial polarization behavior, despite their strong influence on the conductivity and rheological behavior of the system.

A similar conclusion can be drawn based on the M" analysis. The electric modulus M" shows an increase of the peak magnitude M''_{peak} and of the conductive relaxation time τ_σ with the S/M ratio. This can be explained by the excess of surfactant that reduces the droplet interconnectivity, leading to more localized charge transport (i.e. higher M_{peak}) and slower relaxation of the electric field.

Effect of MXene concentration

The increase of MXene bulk concentration at fixed S/M ratio mainly leads to two effects on the sample structure: a decrease of the droplet size and an increase of the droplet aspect ratio (Figure 5b and c). The decrease in droplet size was also reported in studies on emulsion-templated MXene aerogels.[6,9] This decrease can be attributed to the increase of interfacial coverage that arrests droplet coalescence and, therefore, promotes the stabilization of smaller droplets.[51] The increase of the aspect ratio is also caused by the increase of interfacial

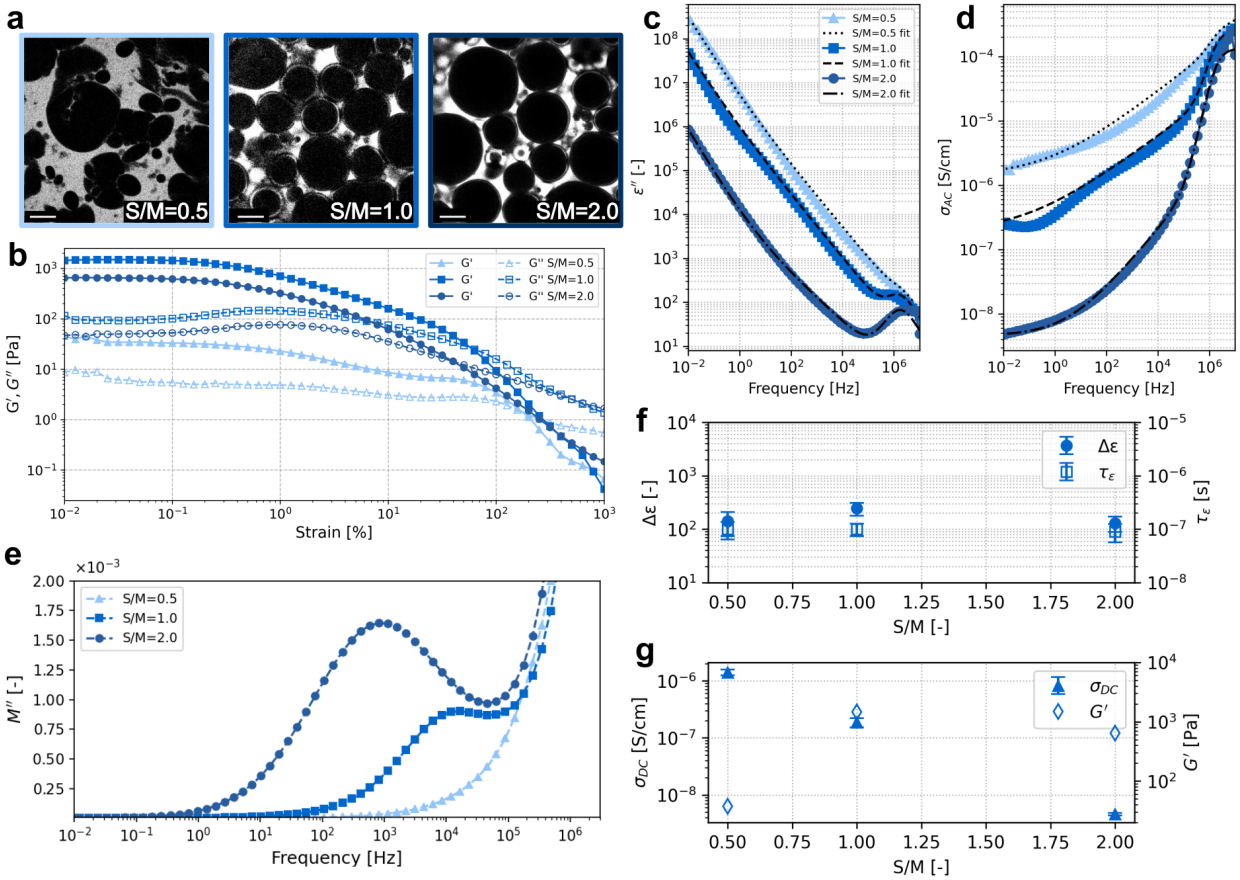

Figure 4: Water-dodecane emulsions with 5 mg/mL of MXenes and $\phi_w = 0.70$ at different S/M (S=$PDMSNH_2$ - M=$Ti_3C_2T_X$). (a) Confocal images. Scale bar is 100 μm. (b) Shear amplitude sweep at $\omega = 1\ rad/s$. (c) Dielectric loss ε'' and (d) AC conductivity σ_{AC} versus frequency. The lines represent the fits obtained from Eq. 1. (e) Electric modulus M" versus frequency. (f) Dielectric strength $\Delta\varepsilon$, dielectric relaxation time τ_ε and (g) DC conductivity σ_{DC} obtained from Eq. 1 together with the LVE storage modulus G' at 1 rad/s as a function of S/M ratio. The error bars correspond to model uncertainty derived from the parameter covariance matrix of the nonlinear least-squares fit in Eq. 1.

coverage. On one hand, a higher particle density leads to significant interfacial instabilities during droplet breakup (e.g. in the emulsion mixing phase) leading to the formation of daughter droplets with a jammed interface that mantain an anisotropic shape even after flow cessation.[18,23] On the other hand, the increase of interfacial coverage can also promote arrested coalescence and, once again, the formation of anisotropic droplets.[52] Overall, both the decrease in droplet size and increase in aspect ratio promote the formation of a higher total interfacial area that leads to a more interconneted droplet network.

These macrostructural changes appear to have a limited effect on the viscoelastic properties of the emulsion (Figure 5d). Studies on the effect of particle concentration on the rheological properties of Pickering emulsions mostly focused on emulsions stabilized by spherical particles, where the particles are shared by the interfaces of multiple droplets acting as bridges between them.[51,53,54] In such cases, the gel strength is mainly determined by the fraction of bridging particles and therefore increases with the increase of particle concentration in the bulk phase. In contrast, for MXene-stabilized emulsions, the high aspect ratio and strong hydrophobicity of the MXene sheets are unlikely to favor particle bridging between droplets. Consequently, increasing the bulk MXene concentration primarily enhances the interfacial stiffness of individual droplets but does not significantly improve interdroplet connectivity. As a result, the viscoelastic moduli of the emulsion are expected to show little dependence on particle concentration.

Conversely, the structural changes have a clear effect on the dielectric and conductive properties. When the MXene concentration is above 10 mg/mL, the dielectric response is dominated by the conductive contribution with σ_{DC} increasing with the particle concentration (Figure 5). The results match the conductivity values by Cao et al.[6] of emulsion-templated MXene porous composites with σ_{DC} up to 10^{-6} S/cm for 5 mg/mL of MXenes in the bulk phase. This also suggests that the main contribution to the electrical transport comes from the interfacial network and not from the dispersed MXenes in the bulk phase.

The high conductivity contribution makes it difficult, at these concentrations, to distin-

guish the dielectric and relaxation processes as done for the emulsions prepared at 5 mg/mL MXene concentration. Nonetheless, consistent with the interfacial measurements in Figure 1, the increase of MXene bulk concentration leads to the formation of a more conductive emulsion network (Figure 5g). Therefore, the increase in bulk conductivity can be attributed to the combination of a more conductive interfacial film and an increase in total interfacial area generated by the smaller, more elongated droplets. In addition, the relaxation may become less distinguishable because the characteristic interfacial polarization frequency shifts to higher frequencies as the conductivity of the interfacial layer increases. Such a shift has been predicted in numerical studies of coated or core-shell particles, where increasing shell conductivity reduces the relaxation time and moves the dielectric relaxation peak toward higher frequencies.[55] Therefore, at higher MXene concentrations, the relaxation process may partially move outside the experimentally accessible frequency window or overlap with other conductive contributions, making it more difficult to resolve. However, it is important to note that while an increase in interfacial area leads to an increase in conductive pathways, it may also increase the overall contact resistance due to an increased amount of droplet-droplet contacts for smaller droplets. Larger droplets, in contrast, can provide longer continuous pathways with fewer junctions. A quantitative description of these competing effects would require a detailed investigation of the three-dimensional structure of the emulsion network, which is not possible in the present system because of the limited penetration depth of confocal microscopy.

Effect of structure rearrangement on conductivity under shear

The effect of shear on the conductivity of the emulsions was investigated by performing a shear amplitude sweep while measuring the dielectric properties at a frequency of 1 Hz (Figure 6a). The conductivity remains constant until a strain of approximately 10%, followed by a decrease at higher strains. This decrease in conductivity can be attributed to the rearrangement of the droplets under shear, which leads to a decrease in the number of conductive

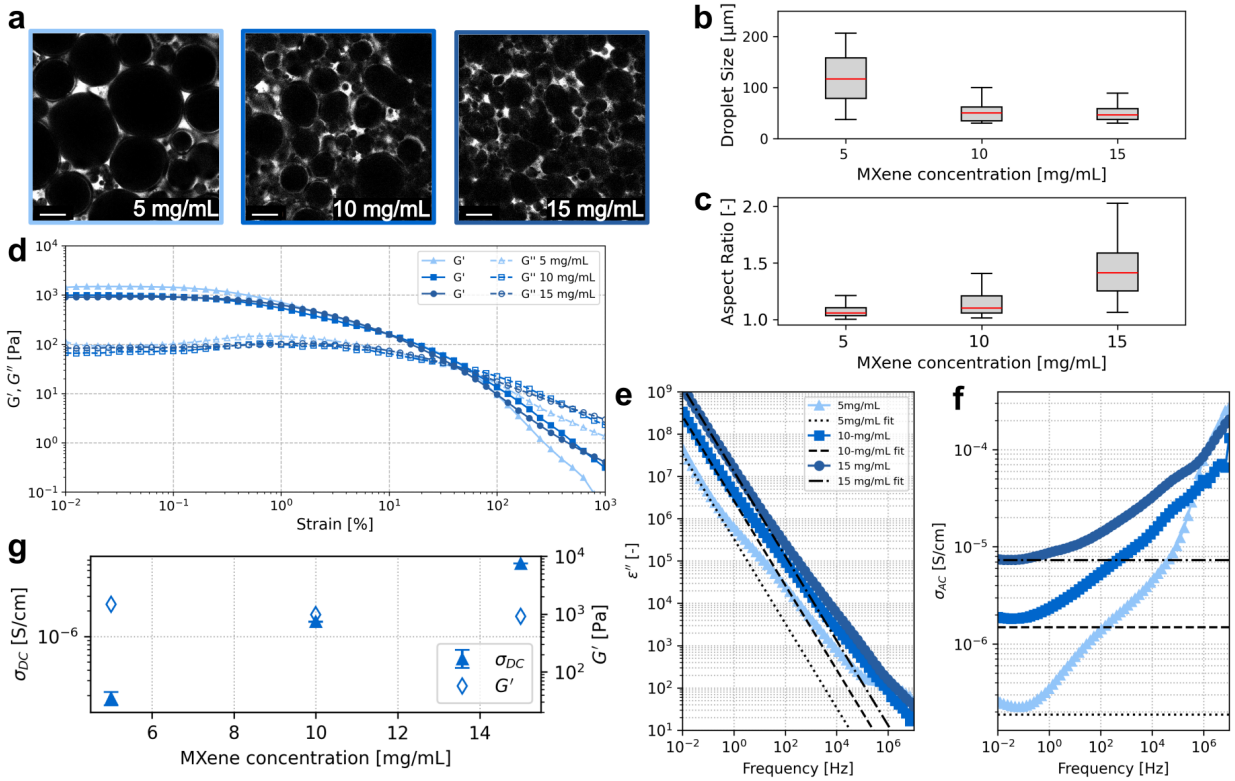

Figure 5: Water-dodecane emulsions with water volume fraction $\phi_w = 0.70$ and S/M=1 (S=PDMSNH$_2$ - M=$Ti_3C_2T_X$) for different MXene bulk concentrations between 5 and 15 mg/mL. (a) Confocal images. Scale bar is 100 μm. (b) Droplet size and (c) aspect ratio versus MXene concentration. (d) Shear amplitude sweep at $\omega = 1\ rad/s$, (e) Dielectric loss and (f) AC conductivity σ_{AC} versus frequency. The lines represent the conductivity contribution. (g) DC conductivity σ_{DC} obtained from Eq. 1 together with the LVE storage modulus G' at 1 rad/s as a function of MXene concentration. The error bars correspond to model uncertainty derived from the parameter covariance matrix of the nonlinear least-squares fit in Eq. 1.

pathways in the emulsion. To assess the origin of this rearrangement, we performed the same amplitude sweep while imaging the emulsion structure using a rheo-optical setup. At low strain, the droplets are closely packed and move as a solid-like material without any visible rearrangement. At the very end of the conductivity linear region ($\gamma = 6.3\%$), intracycle rearrangement of droplets is observed with droplets sliding and rolling over each other (see Movie S1). However, these rearrangements are reversible and the droplets return to their original location at the end of every cycle. At higher strains ($\gamma = 10\%$), a loss of droplet-droplet contacts is observed within cycles, leading to a decrease of the number of conductive pathways and a drop in conductivity (see Figure 6b and Movie S2). When $\gamma \geq \gamma_{crossover}$, the droplets undergo significant irreversible rearrangements as shown in Figure 6c and Movie S3. A similar behavior was observed by Hermes et al. in their study on silica-stabilized oil-in-water emulsions.[56] At low strain, the droplets are trapped in the cages formed by their neighbours and not able to drastically rearrange. When droplets escape from the neighbour cages, irreversible rearragement can be noticed. These dynamics are valid for emulsion systems where droplets have a certain degree of freedom, while in systems like bi-liquid foams (i.e. the droplets are only separated by a thin layer of continuous phase) the droplets undergo irreversible breakage of the structure, such as thin film rupture and droplet coalescence.

It is interesting to notice that, for our samples, even at high strains, the droplets act like solid-like particles without significant deformation in the shear direction and also no coalescence phenomena are observed. Low droplet deformation was observed even when continuously shearing the emulsion at $\dot{\gamma} = 100s^{-1}$. According to the findings in our previous study, single MXene-covered droplets deform under shear flow only when the capillary number $Ca = \eta_m R\dot{\gamma}/\Gamma$ is higher than $Ca \approx 0.3$ for systems with viscosity ratio $\lambda = \eta_{droplet}/\eta_{matrix} \approx 10^{-5}$.[23] In the present study, the viscosity ratio is much larger ($\lambda = 0.64$) , which would typically promote greater droplet deformation at comparable Ca values. However, under the shear conditions used here, the capillary number remains extremely low ($Ca \approx 10^{-3}$ at $\dot{\gamma} = 100s^{-1}$), primarily due to the low viscosity of the continu-

ous phase. Together with the strong interfacial rigidity imparted by the MXene nanosheets, which improves droplet mechanical stability, and the confinement effects of dense emulsions, which further limit droplet shape changes under shear, this results in minimal deformation. The high droplet stability enables the bulk network to recover its elasticity after flow cessation, as reflected by the recovery of G', whereas the conductivity reaches about half of its original value (Figure 6d). Notably, both quantities exhibit a similar time-dependent recovery, with a fast initial increase followed by a slower approach to a plateau, indicating that they are governed by the same underlying droplet-network reformation process. This self-recovery behavior is particularly important for applications such as the fabrication of 3D-printed conductive composites, where it is essential to maintain the mechanical and functional properties before and after printing (i.e. flow).

Conclusions

This study provides insight into the mechanisms governing the rheological and electrical properties of MXene-stabilized Pickering emulsions by combining interfacial and bulk measurements. Taken together, the results define a formulation space for tailoring functionality. The conductivity of the emulsion is related to the MXene-PDMSNH_2 interfacial network, whose conductivity increases with MXene concentration and with S/M through enhanced nanosheet connectivity at the interface. However, the macroscopic electrical performance is ultimately governed by how efficiently this interfacial conductivity is transmitted through the droplet network.

Tailoring the emulsion for practical applications requires a balance between interfacial reinforcement and droplet-droplet connectivity. Increasing the S/M ratio strengthens the viscoelastic interfacial layer and improves nanosheet connectivity at the interface, which is beneficial when mechanical stability is the primary design target, for example in printable inks where shape retention is required.[9] However, an excess surfactant can reduce droplet

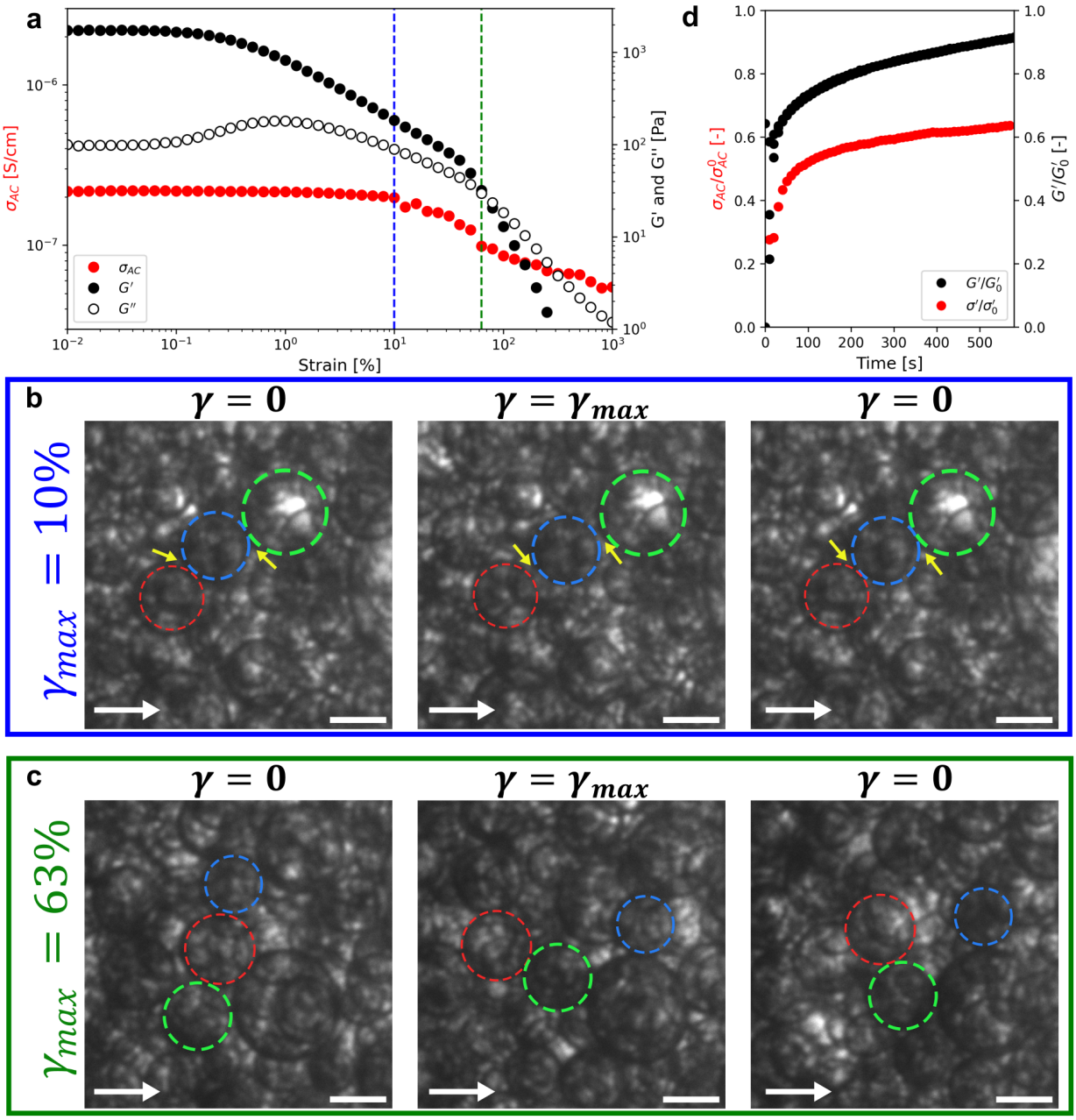

Figure 6: (a) Dynamic moduli and AC conductivity during amplitude sweep measurements at $\omega = 1$ rad/s of an emulsion with 5 mg/mL of MXenes, ϕ_w= 0.70 and S/M=1 (S=PDMSNH$_2$ - M=$Ti_3C_2T_X$). Effect of shear flow on the emulsion microstrucure within one oscillation cycle visualized in the velocity-vorticity plane at (b) $\gamma = 10\%$ and (c) $\gamma = 63\%$. Scale bars are 100 μm, the white arrows indicate the velocity direction. Movies are available in the Supplementary Material. (d) G' and σ_{AC} recovery after shear at 100 s^{-1} normalized by their respective initial values G'_0 and σ^0_{AC}.

connectivity, weakening the droplet network and suppressing bulk conductivity despite the improved interfacial film properties. Such configurations may be advantageous for applications where charge accumulation at isolated interfaces is desirable, such as dielectric or capacitive materials,[40] since electrical transport through the network is limited. In contrast, low S/M ratios preserve droplet-droplet contacts within the emulsion network, enabling more efficient long-range conductive pathways and therefore higher bulk electrical conductivity, although at the expense of a weaker mechanical network. These formulations are therefore more suitable for applications requiring a conductive liquid medium, such as in stretchable electronics.[57]

From a formulation perspective, these findings suggest that moderate or low S/M ratios are preferable when maximizing bulk electrical conductivity, while higher S/M ratios are advantageous when prioritizing interfacial reinforcement or mechanical stability of the emulsion droplets. In addition, increasing the MXene concentration enhances the intrinsic conductivity of the interfacial network and the overall conductive response of the emulsion by increasing the available interfacial area and nanosheet connectivity. Finally, under shear, emulsions exhibit reversible loss of conductivity due to transient rearrangement of droplets, rather than droplet breakup, which facilitates recovery after flow cessation. These relationships advance the fundamental understanding of electrical conductive transport in Pickering emulsions and provide practical guidelines for engineering MXene-based conductive emulsions with tunable interfacial and bulk conductivity for applications in soft conductive composites.

Acknowledgement

This work has received funding from the European Research Council (ERC) under the European Union's Horizon 2020 research and innovation programme: Grant Agreement No. 948739 - PEM-SPrint as well as from Internal Funds KU Leuven under project number

STG/20/035.

Data availability statement

The data that support the findings of this study are openly available in KULeuven RDR at https://doi.org/10.48804/KQMQUS.

Supporting Information Available

The following files are available free of charge.

- SupplementaryMaterial.pdf
- Movie S1: Bulk oscillatory shear experiment at 6.31% strain
- Movie S2: Bulk oscillatory shear experiment at 10% strain
- Movie S3: Bulk oscillatory shear experiment at 63% strain

References

(1) Zhang, T.; Sanguramath, R. A.; Israel, S.; Silverstein, M. S. Emulsion templating: porous polymers and beyond. *Macromolecules* **2019**, *52*, 5445–5479.

(2) Kimmins, S. D.; Cameron, N. R. Functional porous polymers by emulsion templating: recent advances. *Advanced Functional Materials* **2011**, *21*, 211–225.

(3) Lee, S. H.; Hong, J. S.; Lee, S. J. Electrically conductive microcellular foams via high internal phase emulsions. *Current Opinion in Colloid & Interface Science* **2025**, 101939.

(4) Samaniuk, J. R. Dynamics and rheology of 2D particles at fluid–fluid interfaces. *Current Opinion in Colloid & Interface Science* **2024**, *74*, 101857.

(5) Cao, H.; Wang, Y.; Tan, Z.; Harkin, E.; Dasari, S. S.; Lutkenhaus, J. L.; Radovic, M.; Pentzer, E. B.; Green, M. J. Structured Ti3C2Tz MXene-polymer composites from non-aqueous emulsions. *Matter* **2024**, *7*, 1766–1784.

(6) Cao, H.; Wang, Y.; Sarmah, A.; Liu, K.-W.; Tan, Z.; Arole, K. D.; Lutkenhaus, J. L.; Radovic, M.; Green, M. J.; Pentzer, E. B. Electrically conductive porous $Ti_3C_2T_X$ MXene-polymer composites from high internal phase emulsions (HIPEs). *2D Materials* **2022**, *9*, 044004.

(7) Zheng, Z.; Zhao, Y.; Ye, Z.; Hu, J.; Wang, H. Electrically conductive porous MXene-polymer composites with ultralow percolation threshold via Pickering high internal phase emulsion templating strategy. *Journal of Colloid and Interface Science* **2022**, *618*, 290–299.

(8) Pang, H.; Xu, L.; Yan, D.-X.; Li, Z.-M. Conductive polymer composites with segregated structures. *Progress in Polymer Science* **2014**, *39*, 1908–1933.

(9) Li, L.; Deng, Z.; Chen, M.; Yu, Z.-Z.; Russell, T. P.; Zhang, H.-B. 3D printing of ultralow-concentration 2D nanomaterial inks for multifunctional architectures. *Nano Letters* **2022**, *23*, 155–162.

(10) Zhang, Y.; Zhu, G.; Dong, B.; Wang, F.; Tang, J.; Stadler, F. J.; Yang, G.; Hong, S.; Xing, F. Interfacial jamming reinforced Pickering emulgel for arbitrary architected nanocomposite with connected nanomaterial matrix. *Nature communications* **2021**, *12*, 111.

(11) Bian, R.; Lin, R.; Wang, G.; Lu, G.; Zhi, W.; Xiang, S.; Wang, T.; Clegg, P. S.; Cai, D.; Huang, W. 3D assembly of Ti_3C_2-MXene directed by water/oil interfaces. *Nanoscale* **2018**, *10*, 3621–3625.

(12) Zhao, S.; Li, L.; Zhang, H.-B.; Qian, B.; Luo, J.-Q.; Deng, Z.; Shi, S.; Russell, T. P.;

Yu, Z.-Z. Janus MXene nanosheets for macroscopic assemblies. *Materials Chemistry Frontiers* **2020**, *4*, 910–917.

(13) Cain, J. D.; Azizi, A.; Maleski, K.; Anasori, B.; Glazer, E. C.; Kim, P. Y.; Gogotsi, Y.; Helms, B. A.; Russell, T. P.; Zettl, A. Sculpting liquids with two-dimensional materials: the assembly of $Ti_3C_2T_X$ MXene sheets at liquid–liquid interfaces. *ACS nano* **2019**, *13*, 12385–12392.

(14) Cao, H.; Escamilla, M.; Arole, K. D.; Holta, D.; Lutkenhaus, J. L.; Radovic, M.; Green, M. J.; Pentzer, E. B. Flocculation of MXenes and their use as 2D particle surfactants for capsule formation. *Langmuir* **2021**, *37*, 2649–2657.

(15) Blair, V. E.; Celebi, K.; Müllen, K.; Vermant, J. Electrically conductive thin films derived from bulk graphite and liquid–liquid interface assembly. *Advanced Materials Interfaces* **2019**, *6*, 1801570.

(16) Popple, D.; Shekhirev, M.; Dai, C.; Kim, P.; Wang, K. X.; Ashby, P.; Helms, B. A.; Gogotsi, Y.; Russell, T. P.; Zettl, A. All-liquid reconfigurable electronics using jammed MXene interfaces. *Advanced Materials* **2023**, *35*, 2208148.

(17) He, X.; Lu, Q. A review of high internal phase Pickering emulsions: Stabilization, rheology, and 3D printing application. *Advances in Colloid and Interface Science* **2024**, *324*, 103086.

(18) Mei, Y.; Li, G.; Moldenaers, P.; Cardinaels, R. Dynamics of particle-covered droplets in shear flow: unusual breakup and deformation hysteresis. *Soft matter* **2016**, *12*, 9407–9412.

(19) Rodriguez, A. M. B.; Binks, B. P. High internal phase Pickering emulsions. *Current opinion in colloid & interface science* **2022**, *57*, 101556.

(20) De Smedt, S.; Attaianese, B.; Cardinaels, R. Direct ink writing of particle-based multiphase materials: From rheology to functionality. *Current Opinion in Colloid & Interface Science* **2025**, *75*, 101889.

(21) Cui, S.-M.; Hashmi, S.; Li, W.-Q.; Handschuh-Wang, S.; Zhu, C.-T.; Wang, S.-C.; Huang, Y.-F.; Zhu, G.-M.; Stadler, F. J. Rheology of graphene oxide stabilized Pickering emulsions. *Soft Matter* **2023**, *19*, 4536–4548.

(22) Alhabeb, M.; Maleski, K.; Anasori, B.; Lelyukh, P.; Clark, L.; Sin, S.; Gogotsi, Y. Guidelines for Synthesis and Processing of Two-Dimensional Titanium Carbide ($Ti_3C_2T_X$ MXene). *Chemistry of Materials* **2017**, *29*, 7633–7644.

(23) Attaianese, B.; Velpula, G.; Theissen, J.; Sagis, L. M.; Cardinaels, R. Effects of interfacial rheology on shear-induced dynamics of MXene-covered droplets. *Journal of Colloid and Interface Science* **2026**, 140182.

(24) Seok, S.-H.; Choo, S.; Kwak, J.; Ju, H.; Han, J.-H.; Kang, W.-S.; Lee, J.; Kim, S.-Y.; Lee, D. H.; Lee, J. Synthesis of high quality 2D carbide MXene flakes using a highly purified MAX precursor for ink applications. *Nanoscale Advances* **2021**, *3*, 517–527.

(25) Vananroye, A.; Van Puyvelde, P.; Moldenaers, P. Effect of confinement on droplet breakup in sheared emulsions. *Langmuir* **2006**, *22*, 3972–3974.

(26) Kim, S. J.; Choi, J.; Maleski, K.; Hantanasirisakul, K.; Jung, H.-T.; Gogotsi, Y.; Ahn, C. W. Interfacial assembly of ultrathin, functional MXene films. *ACS applied materials & interfaces* **2019**, *11*, 32320–32327.

(27) Zaccone, A. Analytical solution for the polydisperse random close packing problem in 2D. *Powder Technology* **2025**, *459*, 121008.

(28) Zhou, Z.; Hollingsworth, J. V.; Hong, S.; Cheng, H.; Han, C. C. Yielding behavior in

colloidal glasses: comparison between "hard cage" and "soft cage". *Langmuir* **2014**, *30*, 5739–5746.

(29) Fuhrmann, P. L.; Breunig, S.; Sala, G.; Sagis, L.; Stieger, M.; Scholten, E. Rheological behaviour of attractive emulsions differing in droplet-droplet interaction strength. *Journal of colloid and interface science* **2022**, *607*, 389–400.

(30) Wu, B.; Yang, C.; Xin, Q.; Kong, L.; Eggersdorfer, M.; Ruan, J.; Zhao, P.; Shan, J.; Liu, K.; Chen, D.; Weitz, D. A.; Gao, X. Attractive Pickering Emulsion Gels. *Advanced Materials* **2021**, *33*.

(31) Sanatkaran, N.; Zhou, M.; Foudazi, R. Rheology of macro-and nano-emulsions in the presence of micellar depletion attraction. *Journal of Rheology* **2021**, *65*, 453–461.

(32) Kremer, F.; Schönhals, A. *Broadband dielectric spectroscopy*; Springer Science & Business Media, 2002.

(33) Popov, I.; Cheng, S.; Sokolov, A. P. Broadband dielectric spectroscopy and its application in polymeric materials. *Macromolecular Engineering: From Precise Synthesis to Macroscopic Materials and Applications* **2022**, 1–39.

(34) Hao, T. The interfacial polarization-induced electrorheological effect. *Journal of colloid and interface science* **1998**, *206*, 240–246.

(35) Hayward, D.; Pethrick, R. A.; Siriwittayakorn, T. Dielectric studies of heterogeneous phase polymer systems: poly (ethylene oxide) inclusions in polycarbonate-a model system. *Macromolecules* **1992**, *25*, 1480–1486.

(36) Pelster, R.; Simon, U. Nanodispersions of conducting particles: preparation, microstructure and dielectric properties. *Colloid and polymer science* **1999**, *277*, 2–14.

(37) Brosseau, C. Multiphysics advances in analyzing the role of the interfaces and interphases in electrically conductive particle-filled nanocomposites. *Journal of Applied Physics* **2025**, *138*.

(38) Sedrez, P. C.; Sanchez, C. J. N.; da Silva, M. J.; Barbosa Jr, J. R. Dielectric constant of mixtures of carbon dioxide and n-dodecane between 283 K and 343 K. *International Journal of Thermophysics* **2020**, *41*, 26.

(39) Capaccioli, S.; Lucchesi, M.; Rolla, P.; Ruggeri, G. Dielectric response analysis of a conducting polymer dominated by the hopping charge transport. *Journal of Physics: Condensed Matter* **1998**, *10*, 5595.

(40) Bharati, A.; Wübbenhorst, M.; Moldenaers, P.; Cardinaels, R. Dielectric properties of phase-separated blends containing a microcapacitor network of carbon nanotubes: Compatibilization by a random or block copolymer. *Macromolecules* **2017**, *50*, 3855–3867.

(41) Skodvin, T.; Sjöblom, J. Models for the dielectric properties of flocculated w/o-emulsions. *Journal of colloid and interface science* **1996**, *182*, 190–198.

(42) Brosseau, C. *Electromagnetic Heterostructures: Background and Calculation Methods*; Elsevier, 2025.

(43) Belattar, J.; Graça, M.; Costa, L.; Achour, M.; Brosseau, C. Electric modulus-based analysis of the dielectric relaxation in carbon black loaded polymer composites. *Journal of Applied Physics* **2010**, *107*.

(44) Bordi, F.; Cametti, C. Occurrence of an intermediate relaxation process in water-in-oil microemulsions below percolation: the electrical modulus formalism. *Journal of colloid and interface science* **2001**, *237*, 224–229.

(45) Papathanassiou, A. N.; Mykhailiv, O.; Echegoyen, L.; Sakellis, I.; Plonska-Brzezinska, M. E. Electric properties of carbon nano-onion/polyaniline composites: a combined electric modulus and ac conductivity study. *Journal of Physics D: Applied Physics* **2016**, *49*, 285305.

(46) Steeman, P.; Maurer, F. An interlayer model for the complex dielectric constant of composites: an extension to ellipsoidally shaped particles. *Colloid and Polymer Science* **1992**, *270*, 1069–1079.

(47) Lee, K.; Das, M.; Pitell, M.; Wirth, C. L. Surfactant induced catastrophic collapse of carbon black suspensions used in flow battery application. *Journal of Colloid and Interface Science* **2023**, *633*, 712–722.

(48) Das, M.; Lee, K.; Wirth, C. L. Surfactant-Driven Dynamic Changes in Rheology of Activated Carbon Slurry Electrodes. *ACS Applied Materials & Interfaces* **2024**, *16*, 42049–42058.

(49) Perumal, S.; Atchudan, R.; Lee, W. A review of polymeric micelles and their applications. *Polymers* **2022**, *14*, 2510.

(50) Prabhu, V. M.; Venkataraman, S.; Yang, Y. Y.; Hedrick, J. L. Equilibrium self-assembly, structure, and dynamics of clusters of star-like micelles. *ACS Macro Letters* **2015**, *4*, 1128–1133.

(51) Kaganyuk, M.; Mohraz, A. Non-monotonic dependence of Pickering emulsion gel rheology on particle volume fraction. *Soft Matter* **2017**, *13*, 2513–2522.

(52) Kaganyuk, M.; Mohraz, A. Impact of particle size on droplet coalescence in solid-stabilized high internal phase emulsions. *Langmuir* **2019**, *35*, 12807–12816.

(53) Lee, M. N.; Chan, H. K.; Mohraz, A. Characteristics of pickering emulsion gels formed by droplet bridging. *Langmuir* **2012**, *28*, 3085–3091.

(54) Tiwari, M.; Basavaraj, M. G.; Dugyala, V. R. Pickering Emulsions: Role of Particle Wettability and Adhesive Force on Droplet Bridging. *Langmuir* **2024**, *40*, 26474–26486.

(55) Fourn, C.; Lasquellec, S.; Brosseau, C. Finite-element modeling method for the study of dielectric relaxation at high frequencies of heterostructures made of multilayered particle. *Journal of Applied Physics* **2007**, *102*.

(56) Hermes, M.; Clegg, P. S. Yielding and flow of concentrated Pickering emulsions. *Soft Matter* **2013**, *9*, 7568–7575.

(57) Wang, Q.; Ji, X.; Liu, X.; Liu, Y.; Liang, J. Viscoelastic metal-in-water emulsion gel via host–guest bridging for printed and strain-activated stretchable electrodes. *ACS nano* **2022**, *16*, 12677–12685.

TOC Graphic

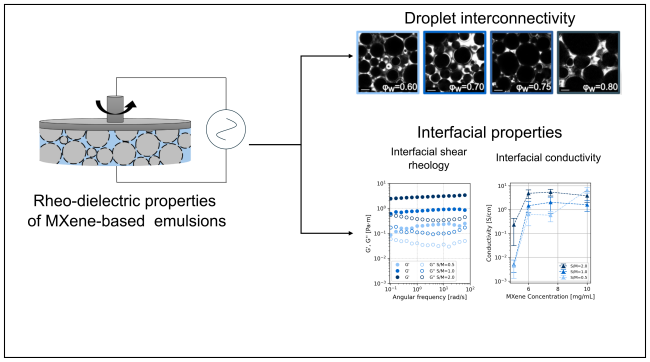
Droplet interconnectivity
φ_W=0.60
φ_W=0.70
φ_W=0.75
φ_W=0.80
Interfacial properties
Interfacial shear rheology
Interfacial conductivity
Rheo-dielectric properties of MXene-based emulsions
Angular frequency [rad/s]
MXene Concentration [mg/mL]